1
2
3
4
5
6
7
8
9
10
11
12
13
14
15
16
17
18
19
20
21
22
23
24
25
26
27
28
29
30
31
32
33
34
35
36
37
38
39
40
41
42
43
44
45
46
47
48
49
50
51
52
53
54
55
56
57
58
59
60
61
62
63
64
65

Supercapacitor electrodes by direct growth of multi-walled carbon nanotubes on

Al: a study of performance versus layer growth evolution

Fu Zhao[a,I], Antonello Vicenzo[a,*,†] Mazdak Hashempour[a], Massimilano Bestetti[a]

([a]) Politecnico di Milano, Dipartimento di Chimica, Materiali e Ingegneria Chimica

"Giulio Natta", Via L. Mancinelli 7, 20131 Milano, Italy

([I]) Current address: Department of Materials Science & Engineering, University of Virginia,

395 McCormick Road, Charlottesville, VA 22904-4745

(†) ISE Member

* Corresponding author

Dipartimento di Chimica, Materiali e Ingegneria Chimica "Giulio Natta",

Politecnico di Milano, Via L. Mancinelli 7, 20131 Milano, Italy. Tel.: +39 02

23993140; fax: +39 02 23993180.

antonello.vicenzo@polimi.it

1

Abstract

Supercapacitor electrodes were fabricated by direct growth of multi-walled carbon nanotubes (CNTs) on Al current collectors via a chemical vapor deposition process in the presence of a spin-coated Co-Mo catalyst. A detailed study of the dependence of the CNT layer structure and thickness on growth time set the basis for the assessment of supercapacitors assembled with the CNTs/Al electrodes. As the main features of the layer growth evolution, an increase in the population of finer CNTs and a shift from a random entanglement to a rough vertical alignment of nanotubes were noted with proceeding growth. The growth time influence on the performance of supercapacitors was in fact apparent. Particularly, the specific capacitance of CNTs/Al electrodes in 0.5 M K_2SO_4 aqueous electrolyte increased from 35 to 80 F g^{-1} as the CNT layer thickness varied from 20 to 60 µm, with a concurrent loss in rate capability (knee frequency from 1 kHz to 60 Hz). The latter was excellent in general, arguably due to both a fast ion transport through the interconnected CNT network and a negligible contribution of the active layer / current collector contact to the equivalent series resistance (0.15-0.22 mΩ g), a distinct advantage of the direct growth fabrication method. Overall, a relatively simple process of direct growth of CNTs on Al foils is shown to be an effective method to fabricate supercapacitor electrodes, notably in the absence of special measures and processing steps finalized to a tight control of nanotubes growth and organization.

2

1. Introduction

Electrochemical capacitors (ECs), also known as ultra-capacitors or supercapacitors, are an important and rapidly growing class of devices, with widespread application in areas including hybrid vehicles, consumer electronics, medical electronics, power back-up, and load leveling [1-5]. The last decade has witnessed an immense growth in research related to ECs, mainly oriented towards the design and development of novel electrode materials and nanostructures to improve on device performance. Historically, carbon materials have played an important role in ECs, and commercial devices based on activated carbon (AC) have been successfully developed. Unfortunately, the high surface area (1000-2000 m^2g^{-1}) of AC is due to the presence of a high fraction of micropores, which leads to low electrode accessibility and limits the EC performance especially in terms of power density [6,7]. To overcome this limitation, significant efforts have been directed towards the design of nanostructured carbon with high active surface area, tunable porosity, chemical stability and electrical conductivity. Among the family of carbon nanostructures, carbon nanotubes (CNTs) have gained wide popularity as a promising electrode material for a new generation of ECs, due to such properties and features as high electronic conductivity and electrochemical stability, narrow pore size distribution and highly accessible surface area [8-11]. In particular, EC electrodes based on CNTs have been extensively studied [12-17], revealing that significant improvements in device performance are within reach, in terms of both specific capacitance –achieving an order of magnitude increase from about 30 to 300 F g^{-1} in aqueous electrolytes via chemical oxidation of MWCNT surfaces [18]– and power capability –demonstrating the possibility of over two order-of-magnitude enhancement of power density compared to conventional ECs [12,19-20]. In particular, it has been widely recognized that the CNT layer

3

should preferably be in intimate contact with the current collector to ensure mechanical integrity and low contact resistance. In this respect, the direct growth of CNTs on the current collector has been proposed as a straightforward approach as well as an opportunity towards process simplification compared to post-transfer methods [21-23]. Attempts in this direction were performed by growing CNTs directly on metallic substrates, such as nickel [24,25], stainless steel [26,27], Inconel 600 [28,29], and tantalum [30,31]. As a current collector for ECs, aluminum is of greater interest owing to, apart from economic considerations, low mass density, high electrical conductivity and flexibility. However, to date, only a few investigations have been devoted to CNT direct growth by thermal CVD on Al [19,32,33-35], due to the low melting point of the metal (660.8 °C) vis-à-vis the temperature range typical of the CNT growth by CVD. In addition to the low temperature constraint, the deposition of the catalyst film on aluminum and its processing can be intricate [33,36]. Upon substrate heating, inter-diffusion and interaction between the catalyst and the aluminum substrate –which has notoriously a high metallurgical reactivity– can cause catalyst poisoning, precluding nanotube growth. To prevent the inter-diffusion and interaction between catalyst and substrate, an intermediate buffer layer, such as Al_2O_3, TiN or TiO_2, etc. [37,38], is usually deposited on the substrate prior to the catalyst layer deposition. For example, Reit et al. [19] deposited a thin Ni/Ti layer on Al by thermal evaporation; Dörfler et al. [35] used a thin dip-coated Al_2O_3 film on Al as the barrier layer, obtaining dense vertical aligned CNT films. Though the engineering of the substrate surface is a fundamental step towards the effective control of CNT growth –in particular for growing array of vertically aligned CNTs–, it will inevitably increase the complexity of the process and the manufacturing costs. Besides, the extent of performance improvement that can be achieved by this

4

approach has yet to be clarified in detail, notwithstanding the fact that some of proposed solutions may actually be controversial (e.g., a dielectric material, like Al_2O_3, used as the buffer layer is liable to increase the ESR and may impair CNTs/substrate adhesion).

Accordingly, continuing along the research directions outlined above, the objective of the present work was the study of a relatively simple and scalable atmospheric pressure CVD method for the growth of CNTs on Al foils in the absence of a buffer layer between the substrate and the catalyst film. As the catalyst precursor, a relatively thick Co-Mo oxide layer (~50 nm instead of few nm) was deposited directly on the Al substrate by spin coating. The evolution of the CNT population with the growth time was characterized in terms of the CNT diameter distribution and mass density. A comparative study of the electrochemical behavior of ECs fabricated with Al/CNTs electrodes at varying thickness of the CNT layer is presented. The parameters that influence the properties of the resulting ECs are discussed.

2. Experimental details

2.1. Sample preparation

The Al foil (250 μm thick, 2×2 cm^2), which served as the substrate for CNT growth, was subjected to chemical polishing by immersion in an 65% HNO_3 and 98% H_3PO_4 solution (volume ratio 3:17), at 85°C, and subsequently in 1 M NaOH solution, at room temperature. In turn, the as-polished Al foil was thoroughly washed with distilled water in an ultrasonic bath and then immersed in ethanol. By this treatment an average roughness R_a of about 8 nm and a peak-to-valley height R_p of 20 nm were achieved, with almost one order of magnitude improvement in surface smoothness over the pristine surface (R_a 65 nm, R_p as high as 300 nm), as determined by contact

mode Atomic Force Microscopy sampling an area of 50 µm × 50 µm with an NT-MDT Solver SPM instrument.

The Co-Mo catalyst was deposited on polished Al foils by spin-coating, using an ethanol-based precursor solution containing Co and Mo acetate. Table 1 reports the optimum composition of the solution and key parameters of the spin coating process.

< Table.1 >

After drying in air at ambient temperature, the pre-coated Al foils were calcined in an open furnace at 400°C for 5 min.

MWCNTs were directly grown on as-prepared Al foils by CVD in a horizontal quartz tube furnace, using ethylene (C_2H_4) as the carbon precursor gas. The furnace was purged with 1000 sccm N_2 for 5 min before heating up to the growth temperature of 650°C. Once the temperature was stabilized, as-prepared Al foils were mounted on a quartz sheet and inserted into the quartz tube furnace. Subsequently a mixture of 100 sccm N_2 and 25 sccm H_2 was fed to the quartz tube for 5 min to reduce the calcined Co-Mo catalysts. C_2H_4 was introduced in the quartz tube at 50 sccm flow rate, after completion of the catalyst pretreatment. CNTs growth was terminated by purging the quartz tube with a flow of 1000 sccm N_2 for 5 min, then letting the quartz tube to cool down to room temperature under N_2 flow of 50 sccm. The mass loading of MWCNTs on Al was adjusted by varying the growth time in the range from 30 s to 1 h. The mass of MWCNTs on Al foils was measured from the mass difference before and after CNTs deposition by using a Sartorius M2P electronic microbalance with an accuracy of 0.001 mg.

2.2.   CNT characterization

Scanning Electron Microscopy (SEM) (Zeiss EVO-50 microscope) was utilized to

6

analyze the morphology of as-grown CNT layers. The microstructure of as-grown CNTs was examined by high-resolution transmission electron microscopy (HRTEM, Philips CM200-FEG). Thermogravimetric analysis (TGA) and differential thermogravimetry (DTG) were carried out to investigate the purity of as-grown CNTs in a DSC-TGA apparatus (SDT Q600) under air atmosphere from ambient temperature up to 900°C with a heating rate of 5°C min^{-1}. The as-grown CNTs layers were peeled off by using a blade, and the effect of growth time on the porous texture characteristics of CNT layers was investigated by analysis of nitrogen cryo-adsorption isotherms. The nitrogen adsorption measurements at 77.35 K were carried out using a volumetric adsorption apparatus (ASAP 2010M, Micrometrics Instrument Corp.). Nitrogen dose amount for every measured point was set at 3cc STP (standard temperature and pressure, 273 K and 10^5 Pa). The measured relative partial pressure range (p/p^0, actual gas pressure p divided by the vapor pressure p^0) was 0.01 to 1, and three transducers were used to precisely record the pressure change. The pore size distribution of as-grown CNT mats was calculated by using the Barret-Joyner-Halenda (BJH) analysis [39], in the mesopore and macropore ranges, and the model of Dunbin-Astakhov [40], in the micropore range.

2.3.   *Electrochemical measurements*

The as-prepared CNTs/Al samples were punched into round disks with a 12 mm diameter circular die and directly used as electrodes for ECs without any further treatment. All measurements were carried out in a flat cell consisting of two Au-coated copper end contacts and a Teflon body as schematically shown in Fig.1. A cellulose-type separator (thickness 25 μm) was placed between two identical MWCNTs/Al electrodes. 0.5 M K_2SO_4 was used as the electrolyte.

< Fig.1 >

Cyclic voltammograms (CV) were obtained at 5, 10, 20, 50 and 100 mV s^{-1} scanning

the potential in the range 0 to 0.7 V. The electrochemical impedance spectroscopy

(EIS) measurements were performed at open circuit potential (OCP) using a 10 mV

excitation signal, in the frequency range from 10 kHz to 100 mHz, sampling 10 points

per decade. The galvanostatic charge/discharge (CDC) tests were carried out with

specific current ranging from 0.4 to 1 A g^{-1} (with respect to CNTs mass on single

electrode). All electrochemical experiments were carried out using a Solartron 1285

potentiostatic interface coupled with a frequency response analyzer (FRA, Solartron

1296).

3. Results and discussion

3.1 Growth of MWCNT layers on Al

Fig.2-a shows the SEM image of Co-Mo catalyst film calcined and subsequently

reduced in hydrogen atmosphere, prior to the introduction of the carbon precursor gas.

As shown, the Co-Mo catalyst nanoparticles appear uniformly distributed on the Al

foil. The size distribution of the catalyst nanoparticles, assessed by sampling a large

number of nanoparticles (about 500), is shown in the inset of Fig.2-a. The most

frequent particle size is in the range 5 to 15 nm, which is effective for MWCNT

growth. However, the relatively large particle size distribution, in the range of 5 to 40

nm, is expected to affect significantly the CVD growth, namely by inducing a

corresponding size dispersity of CNT diameter.

< Fig.2 >

After the activation of Co-Mo catalyst nanoparticles by the pretreatment in H$_2$

atmosphere, the ethylene gas is introduced into the reactor for CNT growth. The

8

evolution of the surface morphology of CNT layers with the growth time was investigated by ex-situ SEM observations; further, shape and size of individual CNTs taken from the layer surface were observed by HR-TEM. As seen in Fig.2-b, upon exposure to ethylene for 30 s, some catalyst particles appear wrapped in a carbon shell, as revealed by the TEM image (inset of Fig.2-b), occasionally forming agglomerates, while others have already activated CNT growth. The carbon deposit wrapping catalyst particles is likely an amorphous carbon layer, obviously formed during the exposure time to ethylene, and possibly representing the initial formation step of CNT growth [41]. This observation suggests that the 30 s time frame is too short to allow for the activation of CNT growth on most catalyst particles. With increasing time, as shown in Fig.2-c and d, randomly-oriented CNTs cover the surface uniformly. Apparently, the nanotubes are not straight but crooked, with most of the tips decorated with catalyst particles, revealing a dominant tip-growth mode [42]. As anticipated above, the inset TEM image suggests a large size distribution of nanotube diameter. As the growth time increases further, along with an increment in CNT length, the average nanotube diameter decreases, as seen in the insets of Fig.2-e, f, g and h. The expanding population of small diameter CNTs can be related to the rearrangement of large polycrystalline catalyst particles during CNT growth, as reported in [27], i.e. through elongation in the growth direction (see Fig.2-e inset), and fragmentation due to compressive stress from the graphene walls of the CNTs at the base of the particles (in tip-growth mode) [43,44]. Fragments originating from split particles can then act as secondary catalyst for growing the second generation CNTs. Therefore, the secondary growth of finer CNTs takes advantage of the dominant tip growth mechanism and is seeded on top of the primary larger diameter nanotubes.

The shift of the CNT population towards smaller diameter nanotubes engenders significant changes in the layer structure, which are clearly revealed by the SEM images in Fig.2, and further substantiated by the cross section observation of the layer structure in Fig.3.

The variations revealed in the surface appearance and morphology of the CNT mats, particularly those imaged in Fig.2-g and h, suggest that significant modifications occur in the nanotube arrangement with advancing growth. Notably, the formation of outgrowing CNT bundles is seen for growth time in excess of about 30 min, when the CNT diameter decreases to value below 10 nm, as shown in the inset TEM images of Fig.2-g and h. Fig.3 shows the internal structure of as-grown CNT layers by the tilted-view SEM micrographs of samples at the cutting edges. As a general remark, it is stressed that the CNT layers are strongly adherent to the Al substrate, as the clear-cut edges of samples in Fig.3 suggest. After 2 min growth a thin and non-uniform CNT layer forms on the substrate (Fig.3-a), with nanotubes of varying diameter and length. A uniform coverage is soon revealed as the growth time increased to 5 min (Fig.3-b), with nanotubes evenly distributed over the surface and interlaced together. After 10 min growth (Fig.3-c), an apparently compact CNT film covers the substrate uniformly to a thickness of a few μm. With growth time further increasing to 30 min, the thickness of the CNT mat rapidly reaches about 20 μm (Fig.3-d). At this stage, the majority of nanotubes are randomly entangled with each other into large bundles, giving a foam like appearance and a wavy pattern to the surface. For growth time in excess of 30 min, as shown in Fig.3-e and Fig.3-f, a distinct variation in the layer structure is noticed. The cross-section view clearly reveals layering within the CNT mats and, upon closer examination (see insets in Fig.3-e and Fig.3-f), the presence of bunches of roughly aligned CNTs in the top-layer.

10

Summarizing, as growth proceeds, the CNT arrangement changes progressively from a random interlacing, due to the curved nature of larger diameter CNTs, towards an imperfect alignment of smaller diameter CNTs, which gives rise to straight bundles, separated by empty spaces, sprouting at the layer surface.

Additional information relating to the evolution of CNT growth was gathered by monitoring the change in mass and thickness of CNT layers during growth. Fig.4-a and (b) report the measured CNT layer areal mass density ρ_A (mg cm^{-2}) and the apparent thickness h from SEM observation as a function of growth time t, respectively. From the areal mass density and the apparent thickness, the volumetric density ρ (g cm^{-3}) of as-grown CNT layers can be calculated and it is reported in Fig.4-c. The ρ_A-t relationship, namely cumulative mass kinetics, exhibits a theoretical S-shaped Gompertz growth behavior [45] over the growth time range up to about 20 min (dotted curve in Fig.4-a), after which a linear behavior sets in (dashed line in Fig.4-a). The apparent thickness h displays a nonlinear behavior with time, up to about 20 min, as shown in Fig.4-b; for growth time exceeding 20 min, a linear correlation is established between CNT layer thickness and time. These findings, which are in partial agreement with previous reports [46,47], can be qualitatively matched with the above reported changes in morphology during CNT growth. Significantly, as shown in Fig.4-c, the maximum value of the calculated mass density of about 0.5 g cm^{-3} occurs at 10 min growth time, which apparently correlates with the prevalence of relatively short and thick CNTs in samples grown within this time frame. Longer growth time entails a continuous decrease of the mass density, down to 0.1 g cm^{-3} after 1 h, consistently with a gradually growing population of thinner and longer nanotubes, first appearing, in fact, after 10 min growth time and thereafter regularly seen by TEM, and in coincidence with the self-termination of larger CNTs

11

growth. Moreover, the inclination of finer CNTs towards alignment is likely to further contribute to the observed decreasing mass density by increasing the apparent thickness. Overall, these results, and in particular the difference of kinetics between the initial and later stage of CNT growth, are probably the outcome of both the deactivation and fragmentation of relatively large catalyst particles and the subsequent secondary CNTs generation, in line with the above discussion. Accordingly, the progressive reduction of the growth rate suggested by the variation of the areal density vs. time in Fig. 4-a occurs over the time interval corresponding to the stage of primary CNTs growth termination.

The results of the thermal analysis of CNT samples grown for different time add further insight in this direction. TGA and DTG curves of MWCNTs after 30 min, 45 min and 1 h growth time are shown in Fig.5-a, b and c, respectively. As illustrated in these figures, two stepwise weight loss can be seen. The first combustion stage, over the range from 150 to 450°C, is assigned to the combustion of amorphous carbon (a-C) impurities. These impurities burn away slowly as the temperature increases to 450°C, producing a broad peak in DTG curves at 435°C, which accounts for an a-C mass fraction of approximately 3, 5 and 8.5% in the CNT layer after 30, 45 and 60 min growth, respectively. The distinct peak in DTG curves at 610 °C obviously corresponds to the combustion of CNTs over the range from 450 to 700°C. The detection of an increasing fraction of a-C based impurities with the growth time is consistent with the declining CNT growth rate, as noted above, in the assumption that, as it is commonly believed, amorphous carbon may cause the poisoning of catalyst particles [41].

3.2 Porous texture of as-grown CNTs layers

In view of the progressive change in diameter, arrangement and purity of CNTs with the growth proceeding, distinct textural characteristics of as-grown CNT layers were expected. Fig.6-a shows the N_2 adsorption/desorption isotherms obtained from the CNT layers after 60 min (I), 45 min (II) and 30 min (III) growth time, respectively. Irrespective of the latter, the adsorption isotherms exhibit a similar trend and common features, corresponding to type IV isotherm characteristic of mesoporous adsorbents, according to the IUPAC nomenclature. The multi-stage adsorption process occurring in aggregated CNT mats as described by Yang et al. [48] can be assumed to apply to the present case. The pore size distribution curves in Fig.6-b. show that all the CNT mats have a multiple pore structure indicated by the multimodal distribution curve. The texture characteristics of CNT layers at various growth time are listed in Table 2. With advancing growth, the specific surface area increases from 178 m^2 g^{-1} for sample III, to 261 and 292 m^2 g^{-1} for sample II and I, respectively. This relatively abrupt change in the surface area is accompanied by a similarly steep increase of the micropore volume and, significantly, by a strong reduction of the macropore volume (resulting in a linear change of the relative macropore volume vs. growth time). On the other hand, a variation in the relative mesopore volume is found only for sample I (60 min growth) and it is comparatively less important, with a change of V_{meso}/V_{total} from 0.54 (III) to 0.66 (I). Overall, the above changes are reflected by the reduction of the average pore diameter with the growth time, as reported in Table 2.

3.3 Electrochemical characterization of MWCNTs/Al electrodes

Three types of MWCNTs/Al electrodes –with layer thickness of 60 (I), 40 (II) and 20 µm (III)– were characterized to investigate the influence of the CNTs growth time on

13

the electrochemical performance of their corresponding ECs, namely as-grown CNT

ECs. Fig.7-a shows the CV curves of the as-grown CNT ECs measured at 100 mV s^{-1}.

All the CV curves show a rectangular shape, indicating a nearly ideal capacitive

response [4]. Interestingly, the response gets closer and closer to an ideal one with

decreasing thickness, suggesting, as expected, that a thinner CNT layer leads to a

better dynamic response. On the other hand, as shown in Fig.7-a, the mass-normalized

current I_s (A g^{-1}) decreases with the decrease of CNT layer thickness. Thus the

specific electrode capacitance $C_{s,electrode}$, estimated according to equation (1):

$$C_{s,electrode} = C_{s,cell} \times 4 = (\int I_s\, dV)/\Delta V \nu \times 4 \tag{1}$$

where $C_{s,cell}$ is the specific cell capacitance, I_s is the mass-normalized current (A g^{-1}),

ΔV is the potential window (V) and ν is the potential scan rate (V s^{-1}), decreases from

about 80 F g^{-1} to 35 F g^{-1} with varying CNT layer thickness from 60 to 20 μm.

To emphasize the effect of CNT growth time on the rate capability of the electrodes,

CV curves were measured at various scan rates from 5 to 100 mV s^{-1}. Fig.7-b reports

the dependence of the specific capacitance of these electrodes and their corresponding

ECs on the CV scan rate. All three types of electrodes show a good capacitance

stability with increasing scan rate, a result that can be associated with fast ion

transport through the interconnected 3D hierarchical porous network of as-grown

CNT layers. The best rate performance is obtained for type (III) electrode –due to the

predominantly meso-macroporous structure, thus a comparatively shorter migration

path, and possibly larger electrolyte uptake– while a slight capacitance loss (about

7%) is found for type (I) electrode when the scan rate is raised from 5 to 100 mV s^{-1},

consistently with the observed change in the pore structure of the CNT layer as well

14

as the increased fraction of a-C with growth time. Actually, the build-up of a-C impurities in CNT layers at longer growth time, as shown by TGA results, is expected to negatively affect the rate capability by blocking electron conducting pathways and reducing the interconnected porosity. Moreover, due to high susceptibility of a-C impurities towards electrochemical oxidation [49], further degradation in rate performance might arise as a result of stronger interactions between oxidized CNTs and ionic species.

Fig.8 shows the EIS response of the CNT/Al ECs fabricated with the three types of CNT electrodes. The impedance characteristics of all ECs are very close to ideal. As seen in Fig.8-a, in the low frequency region, the Nyquist plots show quasi-vertical lines, indicating the almost purely capacitive behavior of as-grown CNT ECs. In the high frequency region, none of the three curves show a semicircle, indicating a good electrical contact between the CNT layers and Al current collector, a distinct advantage of the direct growth fabrication method. The ECs also show very small ESR, approximately 0.3 Ω cm^2, regardless of the CNT layer thickness, as a result of the relatively fast ion transport through the interconnected 3D hierarchical CNT network, the high electronic conductivity of CNTs and the direct binder-free contact between CNT layer and Al current collector. The Nyquist plot of the type (III) EC follows the characteristic behavior of a capacitive element over the whole frequency range, showing a straight line with a high slope. Notably, the type (III) EC does not show a Warburg-like behavior in the medium frequency region, revealing the easy electrode accessibility and fast charge-discharge rate expectedly achieved with thin, high purity CNT films. On the contrary, both the ECs assembled with type (I) and type (II) electrodes show a Warburg-like behavior at medium frequency:

15

consequently, the dominant capacitive character of the impedance response is shifted towards higher resistance and lower frequencies.

The frequency at which the deviation occurs, known as knee frequency, defining the frontier between the capacitive and resistive behaviors of the ECs, is useful for assessing the rate capability of electrodes and defining the optimal operation range for the ECs. Precisely, as shown in Fig.8-b, the inflection that marks the transition from the prevailing capacitive behavior at low frequency and the Warburg-like behavior at high frequency is at about 300 Hz and 60 Hz, for the cells assembled with type (II) and type (I) electrodes, respectively. Moreover, the slope of the straight line in the medium frequency range is close to one for type (I) and slightly higher for type (II) EC. These findings, which are in general agreement with the CV results discussed above, confirm that type (I) and (II) electrodes have slightly lower power capability compared to type (III) electrode. This is obviously related to the modifications of the CNT layer pore structure, as the Warburg-like behavior suggests, resulting in a smaller penetration depth of the ac signal into the porous layer.

In order to have a more explicit information about the rate capability of the as-grown CNT ECs, the impedance results can be elaborated in terms of complex capacitance $C(\omega)$ [50]:

$$C(\omega) = C'(\omega) - jC''(\omega) \tag{2}$$

with:

$$C'(\omega) = -Z''(\omega)/\omega|Z(\omega)|^2 \tag{3}$$

$$C''(\omega) = Z'(\omega)/\omega|Z(\omega)|^2 \tag{4}$$

16

where $C'(\omega)$ is the real part of the complex capacitance $C(\omega)$, therefore related to an effective double-layer capacitance in the low frequency limit, and corresponding to the value measured during constant-current discharge. $C''(\omega)$ is the imaginary part of the complex capacitance $C(\omega)$, related to the energy dissipation by an irreversible process during the charge storage.

Fig.8-c and d present the real and imaginary parts of the complex capacitance as functions of frequency, respectively. As shown in Fig.8-c, the frequency dependence of the capacitance becomes more and more important as the thickness of the CNT layer increases. Notably, the ECs with 20 µm CNT layer retain more than half of the effective capacitance up to 1 kHz. This is one order of magnitude higher than the value (100 Hz) recently obtained from high power ECs based on CNT electrodes [12]. The ECs with 40 and 60 µm CNT layers show 50% retention at 300 and 60 Hz, respectively, indicating a loss of rate performance with increasing CNT layer thickness, which is on the other hand counterbalanced by an increased effective capacitance. As shown in Fig.8-d, the imaginary part of the complex capacitance exhibits a maximum at a frequency f_0, from which a characteristic time constant τ_0 ($\tau_0 = 1/f_0$) is derived, marking the transition between capacitive and resistive behavior [51]. Accordingly, the shorter τ_0 is, the faster is the EC frequency response. It can be seen in Fig.8-d that half of the low-frequency capacitance is reached at τ_0. In other words, τ_0 represents the minimum time required to discharge all of the stored energy with an efficiency > 50%. The extremely small τ_0 (1 ms) for type (III) EC confirms the very fast ion absorption/desorption dynamics in the 20 µm thick CNT layer. As the CNTs layer thickness increases, τ_0 increases as well (namely, to 3.33 and 16.6 ms at 40 and 60 µm thickness, respectively) due primarily to the increased pore diffusive

17

resistance. Nevertheless, these values are extremely low compared to those previously reported for activated carbon (8 s) and CNT composites (5 s) based ECs [22].

The excellent characteristics of as-grown CNT ECs can also be observed in galvanostatic charge/discharge measurements. As shown in Fig.9-a, the curves measured at the specific current of 1 A g^{-1} show nearly triangular form with a negligible IR drop, revealing a highly reversible charge discharge process for all three types of ECs.

The specific capacitance of ECs was estimated from charge discharge curves by using the following equation:

$$C_{s,electrode} = C_{s,cell} \times 4 = I/(m\,dV/dt) \times 4 \tag{5}$$

where I is the applied current, m is the total mass of active material in the cell and dV/dt is the slope of the discharge curve after the IR drop. Fig.9-b reports the specific capacitance of as-grown CNT electrodes and their corresponding ECs versus specific current. These values are in good agreement with those obtained from CV measurements. The retention of the specific capacitance is excellent even at high applied specific current, with the exception of the type (I) ECs, for which a slight decrease (about 8%) is found.

To further assess the effect of growth time on the performance of the supercapacitors, the trend of the specific capacitance C_s for as-grown CNT ECs over 5000 cycles of charge-discharge was studied, as shown in Fig.10-a. CV measurements were performed after a given number of charge and discharge cycles and are shown in Fig.10-b, c and d. A high retention of C_s is observed from as-grown CNT ECs. The retention is 91.5%, 94% and 96% for ECs type (I), (II) and (III), respectively. A lower

18

retention obviously correlates with longer growth time, suggesting that the loss of capacitance with cycling is related to the fraction of a-C in the CNT layer.

From galvanostatic charge/discharge curves the specific energy and power density (referred to unit mass of active material in the cell) are deduced by the following equations:

$$E_s = C_{s,cell} \ U^2 \ /2 \tag{6}$$

$$P_s = U^2/4R \tag{7}$$

where $C_{s, cell}$ (F g^{-1}) is the specific capacitance of the EC cell, U (V) is the working potential, excluding the IR drop occurring at the beginning of discharge, and R (mΩ g) is the ESR measured from the IR drop of charge/discharge curves.

Table 3 reports the values of E_s and P_s obtained from this work; these results should be regarded in the light of the small potential range used. The maximum power and energy density of as-grown CNT ECs are 875 kW kg^{-1} and 1.4 Wh kg^{-1}, respectively. Recently, the Dörfler group [35] demonstrated power density of 6.58 MW kg^{-1} and energy density of 8.5 Wh kg^{-1} by operating as-grown vertical aligned CNT-based ECs over a range of 2 V, using an organic electrolyte of tetraethylammonium tetrafluoroborate TEABF$_4$ 0.1 g ml^{-1} dissolved in acetonitrile. According to these authors, the major reason of the low energy density is the nanotubes loose packing in the active layer, resulting in a low density of 0.15-0.4 mg cm^{-2}, which is similar to the CNTs mass load in our work. Apparently, as already noted above, the low temperature operation in CVD, as required for direct growth on aluminum, leads possibly to both inefficient catalyst use and to a progressive deactivation of active catalyst particles and consequently to a low surface density of CNTs. Hence, further

improvement of the storage characteristics of CNTs/Al electrodes is expected by increasing the mass loading, maintaining nonetheless high yield and quality of CNTs, through the optimization of the catalyst preparation and CNT growth conditions. As a further and complementary approach to compensate for the low specific capacitance and energy density, the incorporation of transition metal oxides nanoparticles with pseudocapacitive properties (such as MnO_x) into as-grown CNTs matrix is a promising strategy.

4. Conclusions

A simple approach to fabricate MWCNTs/Al electrodes for supercapacitors is demonstrated by CNT direct growth on aluminum foils via atmospheric pressure catalytic CVD. The growth time dependence of the CNT layer microstructure and the performance of supercapacitors assembled with as-grown CNTs/Al electrodes was addressed.

The CNT growth exhibit a time dependent behavior, notably with changes in both CNT size and arrangement, due to the fragmentation of primary large catalyst nanoparticles and secondary growth. The increasing fraction of finer nanotubes within the CNT population together with the change in the CNT arrangement leads to the decrease of the volumetric mass density of CNTs layers, higher surface area and relative micropore volume.

The electrochemical studies show good to excellent power and energy storage performance using as-grown CNTs coated Al foils as the electrodes for ECs. The specific capacitance of as-grown CNTs/Al electrode increases from 35 to 80 F g^{-1} with the CNT layer thickness increasing from 20 to 60 μm. High rate capability, i.e. relaxation time constant within the millisecond range, are attained in particular with

20

20 μm thick CNT films, thanks to the interconnected 3D hierarchical network structure of the as-grown layer and a very low equivalent series resistance. As a result, a maximum power density of 875 kW kg^{-1} was obtained from the corresponding ECs.

Overall, this work demonstrates that a simple catalytic CVD process for the direct growth of CNTs on Al foils can be an effective method to fabricate electrodes for supercapacitors, notably in the absence of special measures and processing steps finalized to a tight control of nanotubes growth and organization.

Acknowledgements

References

[1]   J.-N. Marie-Françoise, H. Gualous, R. Outbib, A. Berthon, 42 V Power Net with supercapacitor and battery for automotive applications, J. Power Sources 143 (2005) 275.

[2]   B.Y. Ahn, E. B. Duoss, M. J. Motala, X. Guo, S.-I. Park, Y. Xiong, J. Yoon, R. G. Nuzzo, J.A. Rogers, J.A. Lewis, Omnidirectional printing of flexible, stretchable, and spanning silver microelectrodes, Science 323 (2009) 1590.

[3]   J. J. Boland, Flexible electronics: Within touch of artificial skin, Nat. Mater. 9 (2010) 790.

[4]   B.E. Conway, Electrochemical Supercapacitors: Scientific Fundamentals and Technological Applications, Kluwer Academic/Plenum, New York, 1999.

[5]   R. Kötz, M. Carlen, Principles and applications of electrochemical capacitors, Electrochim. Acta, 45 (2000) 2483.

21

[6]   H. Shi, Activated carbons and double layer capacitance, Electrochim. Acta 41 (1995) 1633.

[7]   D. Qu, Studies of the activated carbons used in double-layer supercapacitors, J. Power Sources 109 (2002) 403.

[8]   M. S. Dresselhaus, G. Dresselhaus, P.C. Eklund, Science of Fullerenes and Carbon Nanotubes, Academic Press, New York, 1996.

[9]   R. Saito, G. Dresselhaus, M.S. Dresselhaus, Electronic structure of double-layer graphene tubules, J. Appl. Phys. 73 (1993) 494.

[10]   T.W. Ebbesen, H.J. Lezec, H. Hiura, J.W. Bennett, H.F. Ghaemi, T. Thio, Electrical conductivity of individual carbon nanotubes, Nature 382 (1996) 54.

[11]   J. P. Issi, L. Langer, J. Heremans, C. H. Olk, Electronic properties of carbon nanotubes: Experimental results, Carbon 33 (1995) 941.

[12]   C. Niu, E.K. Sichel, R. Hoch, D. Moy, H. Tennent, High power electrochemical capacitors based on carbon nanotube electrodes, Appl. Phys. Lett. 70 (1997) 1480.

[13]   D. N. Futaba, K. Hata, T. Yamada, T. Hiraoka, Y. Hayamizu, Y. Kakudate, O. Tanaike, H. Hatori, M. Yumura, S. Iijima, Shape-engineerable and highly densely packed single-walled carbon nanotubes and their application as super-capacitor electrodes, Nat. Mater. 5 (2006) 987.

[14]   H. Zhang, G. Cao, Y. Yang, Electrochemical properties of ultra-long, aligned, carbon nanotube array electrode in organic electrolyte, J. Power Sources 172 (2007) 476.

[15]   Y. Honda, M. Takeshige, H. Shiozaki, T. Kitamura, K. Yoshikawa, S. Chakrabarti, O. Suekane, L. Pan, Y. Nakayama, M. Yamagata, M. Ishikawa, Vertically aligned double-walled carbon nanotube electrode prepared by transfer methodology for electric double layer capacitor, J. Power Sources 185 (2008) 1580.

[16]   X. Cui, F. Hu, W. Wei, W. Chen, Dense and long carbon nanotube arrays decorated with Mn_3O_4 nanoparticles for electrodes of electrochemical supercapacitors, Carbon 49 (2011) 1225.

[17]   W. Lu, L. Qu, K. Henry, L. Dai, High performance electrochemical capacitors from aligned carbon nanotube electrodes and ionic liquid electrolytes, J. Power Sources 189 (2009) 1270.

[18]   J.-S. Ye, X. Liu, H. F. Cui, W.-D. Zhang, F.-S. Sheu, T. M. Lim, Electrochemical oxidation of multi-walled carbon nanotubes and its application to electrochemical double layer capacitors, Electrochem. Commun. 7 (2005) 249.

[19]   R. Reit, J. Nguyen, W.J. Ready, Growth time performance dependence of vertically aligned carbon nanotube supercapacitors grown on aluminum substrates, Electrochim. Acta 91 (2013) 96.

[20]   Y. Honda, T. Haramoto, M. Takeshige, H. Shiozaki, T. Kitamura, M. Ishikawa, Aligned MWCNT sheet electrodes prepared by transfer methodology providing high-power capacitor performance, Electrochem. Solid St. Lett. 10 (2007) A106.

[21]   E. Frackowiak, K. Metenier, V. Bertagna, F. Beguin, Supercapacitor electrodes from multiwalled carbon nanotubes, Appl. Phys. Lett.77 (2000) 2421.

[22]   H. Zhang, G.P. Cao, Y.S. Yang, Using a cut-paste method to prepare a carbon nanotube fur electrode, Nanotechnology 18 (2007) 195607.

[23]   C.G. Liu, M. Liu, F. Li, H.M. Cheng, Frequency response characteristic of single-walled carbon nanotubes as supercapacitor electrode material, Appl. Phys. Lett. 92 (2008) 143108.

[24]   B. J. Yoon, S. H. Jeong, K. H. Lee, H. S. Kim, C.G. Park, J. H. Han, Electrical properties of electrical double layer capacitors with integrated carbon nanotube electrodes, Chem. Phys. Lett. 388 (2004) 170.

[25]   N.K. Reddy, J.-L. Meunier, S. Coulombe, Growth of carbon nanotubes directly on a nickel surface by thermal CVD, Mater. Lett. 60 (2006) 3761.

[26]   D. Park, Y. H. Kim, J. K. Lee, Synthesis of carbon nanotubes on metallic substrates by a sequential combination of PECVD and thermal CVD, Carbon 41 (2003) 1025.

[27]   M. Hashempour, A. Vicenzo, F. Zhao, M. Bestetti, Direct growth of MWCNTs on 316 stainless steel by chemical vapor deposition: Effect of surface nano-features on CNT growth and structure, Carbon 63 (2013) 330.

[28]   S. Talapatra, S. Kar, S.K. Pal, R. Vajtai, L. Ci, P. Victor, M.M. Shaijumom, S. Kaur, O. Nalamasu, P. M. Ajayan, Direct growth of aligned carbon nanotubes on bulk metals, Nat. Nanotechnol. 1 (2006) 112.

23

[29]   L.J. Gao, A.P. Peng, Z.Y. Wang, H. Zhang, Z.J. Shi, Z.N. Gu, G.P. Cao, B.Z. Ding, Growth of aligned carbon nanotube arrays on metallic substrate and its application to supercapacitors, Solid State Commun. 146 (2008) 380.

[30]   H. Zhang, G.P. Cao, Z.Y. Wang, Y.S. Yang, Z.N. Gu, Electrochemical capacitive properties of carbon nanotube arrays directly grown on glassy carbon and tantalum foils, Carbon 46 (2008) 822.

[31]   B. Kim, H. Chung, B.K. Min, H. Kim, W. Kim., Electrochemical Capacitors Based on Aligned Carbon Nanotubes Directly Synthesized on Tantalum Substrates, Bull. Korean Chem. Soc. 31 (2010) 3697.

[32]   R. Signorelli, D.C. Ku, J.G. Kassakian, and J.E. Schindall, Electrochemical Double-Layer Capacitors Using Carbon Nanotube Electrode Structures, Proceedings of the IEEE 97.11 (2009) 1837

[33]   V. O. Khavrus, M. Weiser, M. Fritsch, R. Ummethala, M. G. Salvaggio, M.Schneider, M. Kusnezoff, and A. Leonhardt, Application of Carbon Nanotubes Directly Grown on Aluminum Foils as Electric Double Layer Capacitor Electrodes, Chem. Vap. Deposition 18 (2012) 53

[34]   R. Kavian, A. Vicenzo, M. Bestetti, Growth of carbon nanotubes on aluminium foil for supercapacitors electrodes , J. Mater. Sci. 46 (2011) 1487.

[35]   S. Dörfler, I. Felhösi, T. Marek, S. Thieme, H. Althues, L. Nyikos, S. Kaskel, High power supercap electrodes based on vertical aligned carbon nanotubes on aluminum, J. Power Sources 227 (2013) 218.

[36]   S. Dörfler, A. Meier, S. Thieme, P. Németh, H. Althues, S. Kaskel, Wet-chemical catalyst deposition for scalable synthesis of vertical aligned carbon nanotubes on metal substrates, Chem. Phys. Lett. 511 (2011) 288.

[37]   J. J. Nguyen, S. Turano, W. J. Ready, The synthesis of carbon nanotubes grown on metal substrates: A review, Nanosci. Nanotechnol. Lett. 4 (2012) 1123.

[38]   T. de los Arcos, M.G. Garnier, P. Oelhafen, D. Mathys, J.W. Seo, C. Domingo, J.V. Garcia-Ramos, S. Sanchez-Cortes, Strong influence of buffer layer type on carbon nanotube characteristics, Carbon 42 (2004) 187.

[39]   E. P. Barrett, L. G. Joyner, and P. P. Halenda. The determination of pore volume and area distributions in porous substances. I. Computations from Nitrogen isotherms. J. Am. Chem. Soc. 73 (1951) 373.

24

[40] M. M. Dubinin, and V. A. Astahakov, Description of adsorption equilibria of vapors on zeolites over wide ranges of temperature and pressure, Advances in Chemistry, Vol 102, American Chemical Society, 1971; chapter 44, pp 69–85.

[41] C. Schuenemann, F. Schaffel, A. Bachmatiuk, U. Queitsch, M. Sparing, B. Rellinghaus, K. Lafdi, L. Schultz, B. Buechner, M.H. Rummeli, Catalyst poisoning by amorphous carbon during carbon nanotube growth: Fact or fiction?, ACS Nano 5 (2011) 8928.

[42] M. Bedewy, E.R. Meshot, A.J. Hart, Diameter-dependent kinetics of activation and deactivation in carbon nanotube population growth, Carbon 50 (2012) 5106.

[43] M. Moseler, F. Cervantes-Sodi, S. Hofmann, G. Csanyi, A. C. Ferrari, Dynamic catalyst restructuring during carbon nanotube growth, ACS Nano 4 (2010) 7587.

[44] S. Hofmann, R. Sharma, C. Ducati, G. Du, C. Mattevi, C. Cepek, M. Cantoro, S. Pisana, A. Parvez, F. Cervantes-Sodi, A. C. Ferrari, R. Dunin-Borkowski, S. Lizzit, L. Petaccia, A. Goldoni, J. Robertson, In situ observations of catalyst dynamics during surface-bound carbon nanotube nucleation, Nano Lett. 7 (2007) 602.

[45] C.P. Winsor, The Gompertz curve as a growth curve, P. Natl. Acad. Sci. USA 18 (1932) 1.

[46] M. Bedewy, E.R. Meshot, M.J. Reinker, A.J. Hart, Population growth dynamics of carbon nanotubes, ACS Nano 5 (2011) 8974.

[47] J.-M. Ting, K.-H. Liao, Low-temperature, nonlinear rapid growth of aligned carbon nanotubes, Chem. Phys. Lett. 396 (2004) 469.

[48] Q.-H. Yang, P.-X. Hou, S. Bai, M.-Z. Wang, H.-M. Cheng, Adsorption and capillarity of nitrogen in aggregated multi-walled carbon nanotubes, Chem. Phys. Lett. 345 (2001) 18

[49] H.-T. Fang, C.-G. Liu, C. Liu, F. Li, M. Liu and H.-M. Cheng, Purification of Single-Wall Carbon Nanotubes by Electrochemical Oxidation, Chem. Mater. 16 (2004) 5744.

[50] P.L. Taberna, P. Simon, J.F. Fauvarque, Electrochemical characteristics and impedance spectroscopy studies of carbon-carbon supercapacitors, J. Electrochem. Soc. 150 (2003) A292.

[51]   K.S. Cole, R.H. Cole, Dispersion and absorption in dielectrics I. Alternating

          current characteristics, J. Chem. Phys. 9 (1941) 341.

Captions

Table 1. Composition of the catalyst precursor solution and key parameters of the spin coating process

Table 2. Surface area and porous texture characteristics of as-grown CNT layers versus growth time.

Table 3. Properties of CNTs/Al electrodes, at variable thickness of the CNT layer and the corresponding EC parameters and performance.

Fig.1. Scheme of the flat-cell with an inside view of electrode arrangement.

Fig.2. (a) SEM image of Co-Mo catalyst film calcined and subsequently reduced in hydrogen atmosphere prior to the introduction of ethylene; the inset shows the estimated catalyst particles size distribution. (b) to (h): top-view SEM images of CNT films after the introduction of C_2H_4 for different growth time intervals, as indicated; insets show high-resolution TEM images of CNT specimens prepared by scratching the surface of as-grown CNT layers with a blade.

Fig.3. Tilted-view SEM images of the as-grown CNTs layers after different growth time intervals: (a) 2 min, (b) 5 min, (c) 10 min, (d) 30 min, (e) 45 min and (f) 60 min; insets are high magnification SEM images showing details of the layer structure.

Fig.4. (a) Measured CNT films areal density ρ_A (the dotted line represents the fit of Gompertz model to the experimental data; the dashed line is a linear fit to the experimental data); (b) apparent thickness h (the dotted line represents the exponential fit to the experimental data; the dashed line is a linear fit to the experimental data); (c) calculated volumetric density ρ as a function of growth time.

Fig.5. TGA and DTG curves of MWCNTs after 30 min (a), 45 min (b) and 60 min (c) growth time.

Fig.6. (a) N$_2$ adsorption isotherms obtained on various types of CNT layers grown after 60 min (I), 45 min (II) and 30 min (III); (b) pore size distribution presented as plots of differential pore volume against pore diameter derived from the adsorption isotherms by using BJH method [39].

Fig.7. (a) CV curves of the as-grown CNT ECs measured at 100 mV s^{-1}; (b) specific capacitance vs. scan rate.

Fig.8. (a) Nyquist plots of impedance for as-grown CNT ECs with different CNT layer thickness: 60 µm or type (I), 40 µm or type (II), and 20 µm or type (III); (b) expanded view in the high frequency region; the real (c) and imaginary part (d) of the complex capacitance as a function of frequency.

Fig.9. (a) Galvanostatic charge/discharge curves measured at a constant specific current of 1 A g^{-1} of ECs assembled with 60, 40 and 20 µm CNT/Al electrodes; (b) specific capacitance of as-grown CNT electrodes and of the corresponding ECs versus specific current.

Fig.10. (a) Specific capacitance retention against charge/discharge cycle number for as-grown CNT electrodes and their corresponding ECs; CV of ECs assembled with 60 (b), 40 (c) and 20 µm CNT electrodes (d) vs. cycle number.

Table(s) revision

Table 1 Composition of the ethanol-based catalyst precursor solution and spin coating process parameters for catalyst preparation.

Solution	
$Co(C_2H_3O_2)_2 + Mo_2(C_2H_3O_2)_4$ / mM	50
Co : Mo (atomic ratio)	10 : 1
EtOH: Ethylene Glycol (volume ratio)	100 : 1
Spin coating process program	Step 1- 300 rpm, 10s
	Step 2- 3000 rpm, 1 min

Table 2. Textural characteristics of as-grown CNT layers with various growth time.

CNTs layer [#]	growth time [min]	BET area $[m^2\,g^{-1}]$	V_{total} $[cm^3\,g^{-1}]$	V_{micro} $[cm^3\,g^{-1}]$	V_{meso} $[cm^3\,g^{-1}]$	V_{macro} $[cm^3\,g^{-1}]$	D_A [nm]
I	60	292	1.03	0.18	0.68	0.17	8
II	45	261	0.84	0.12	0.44	0.28	10
III	30	178	1.51	0.05	0.81	0.65	20

Table 3 As-grown CNT layers parameters and the corresponding EC performance.

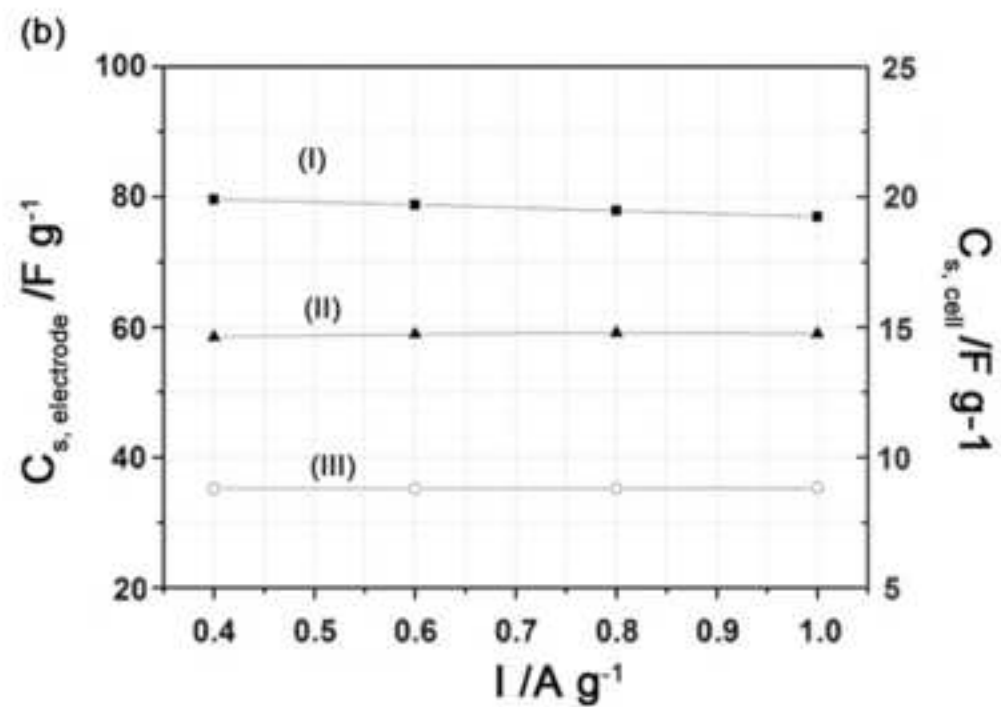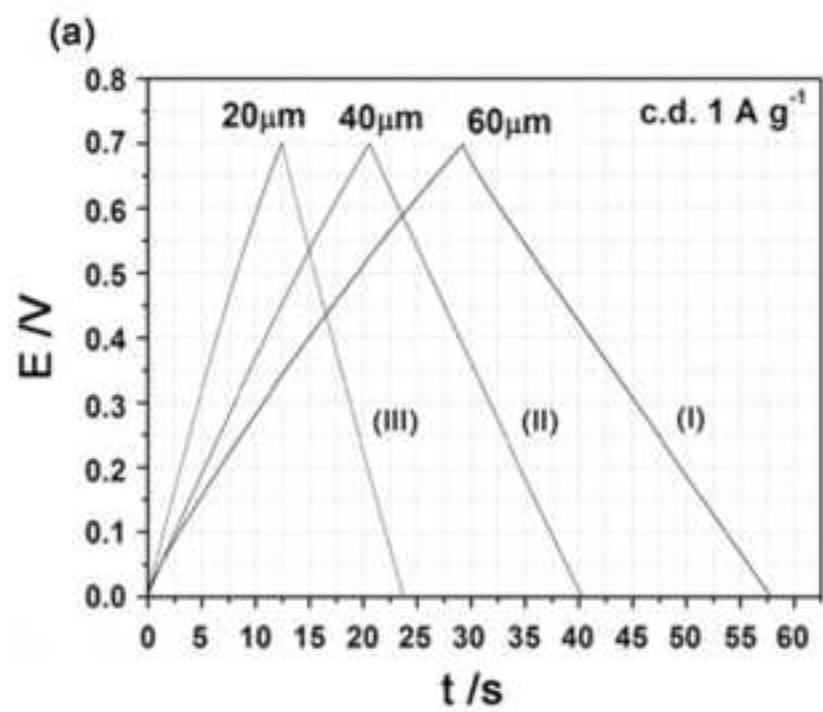| Electrode	I	II	III
Growth time /min	60	45	30
CNT areal density /mg cm^{-2}	0.65	0.48	0.38
Apparent thickness /µm	60	40	20
Electrolyte	0.5 M K_2SO_4		
Working voltage U /V	0.7		
Resistance R_{ESR} /mΩ g	0.22	0.17	0.14
Capacitance $C_{s,\,cell}$ /F g^{-1}	20.7	14.8	8.5
Energy density E_s /Wh kg^{-1}	1.4	1	0.58
Power density P_s /kW kg^{-1}	557	721	875
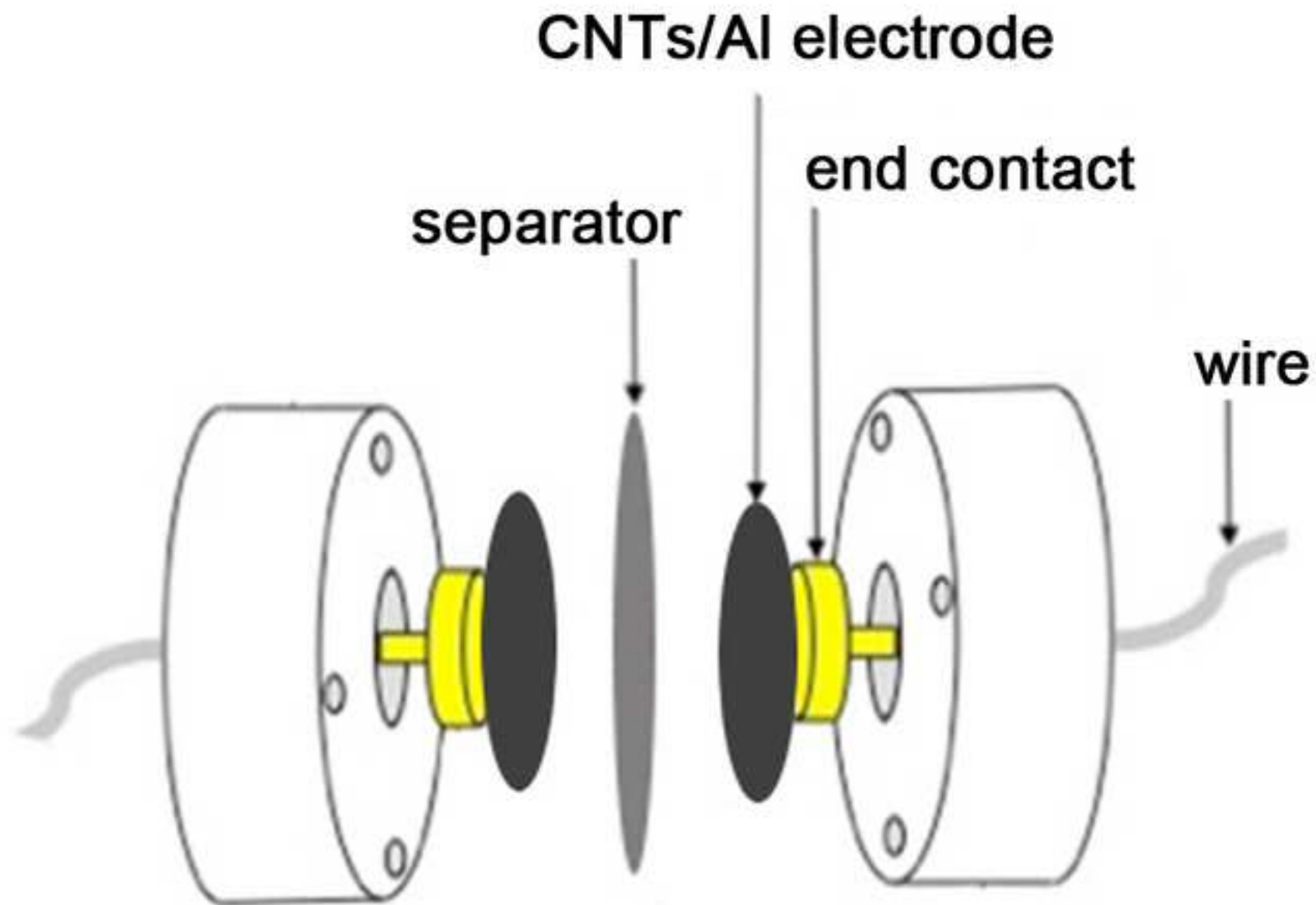
Figure 2
Click here to download high resolution image
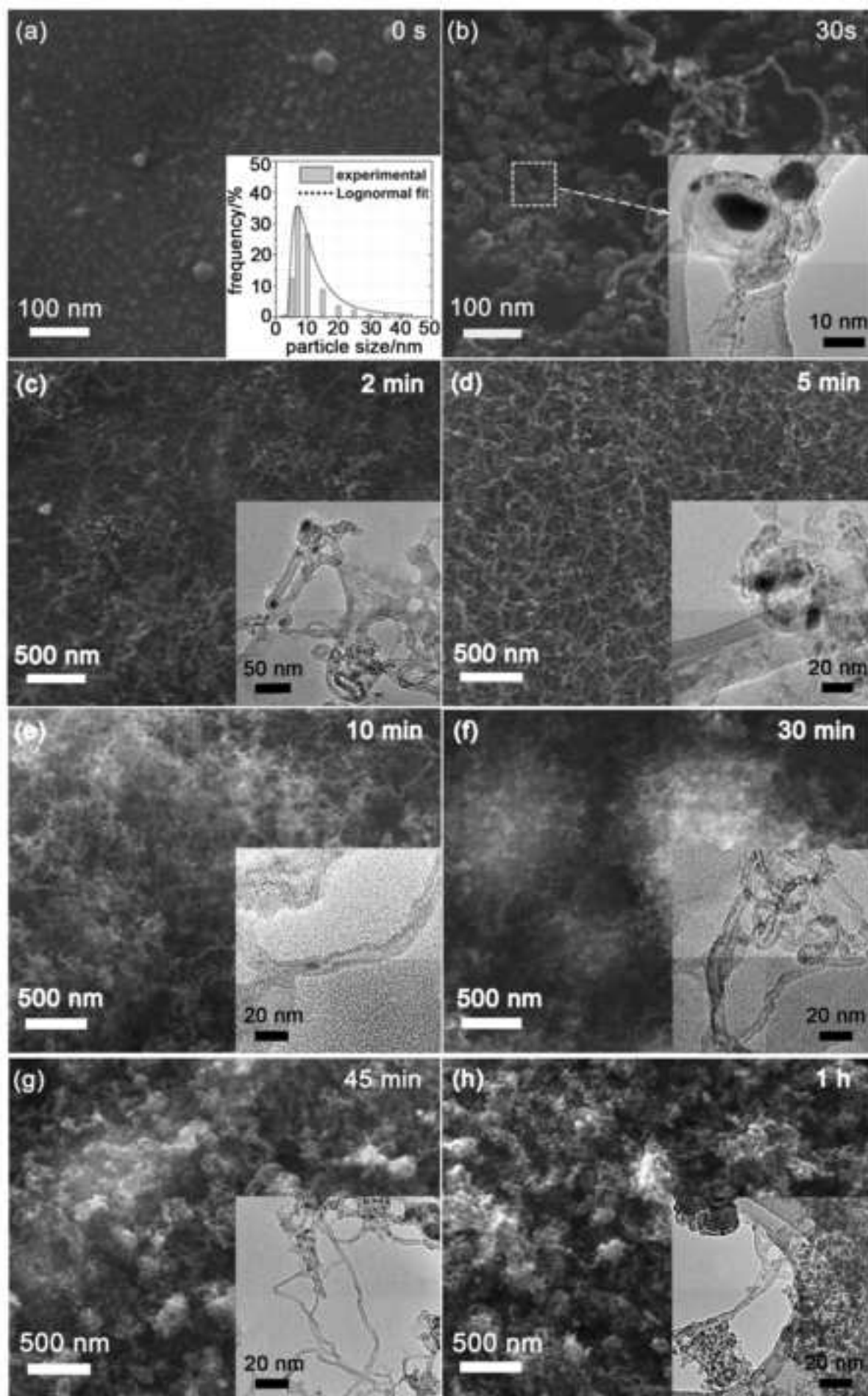
Figure 2

Figure 3
Click here to download high resolution image
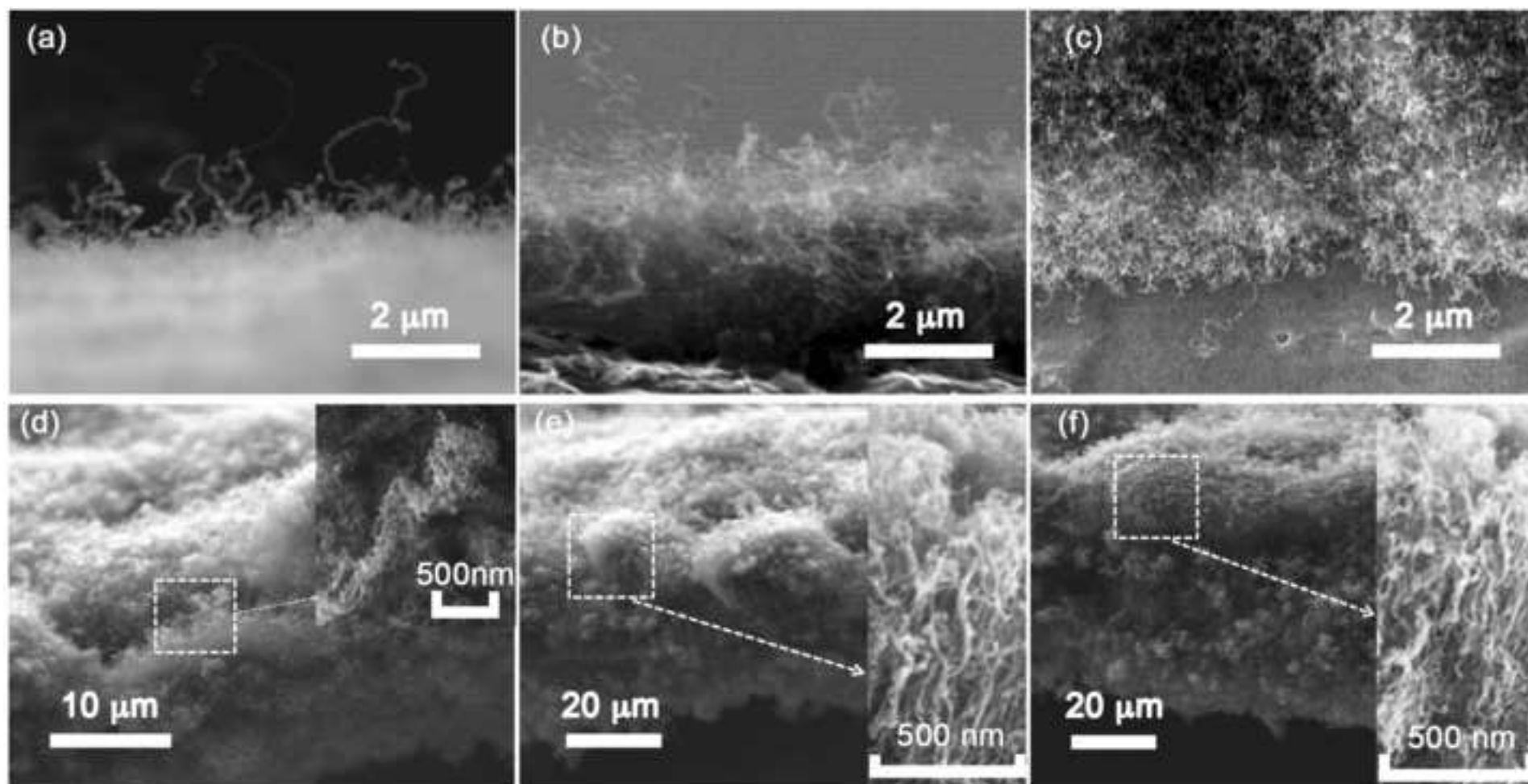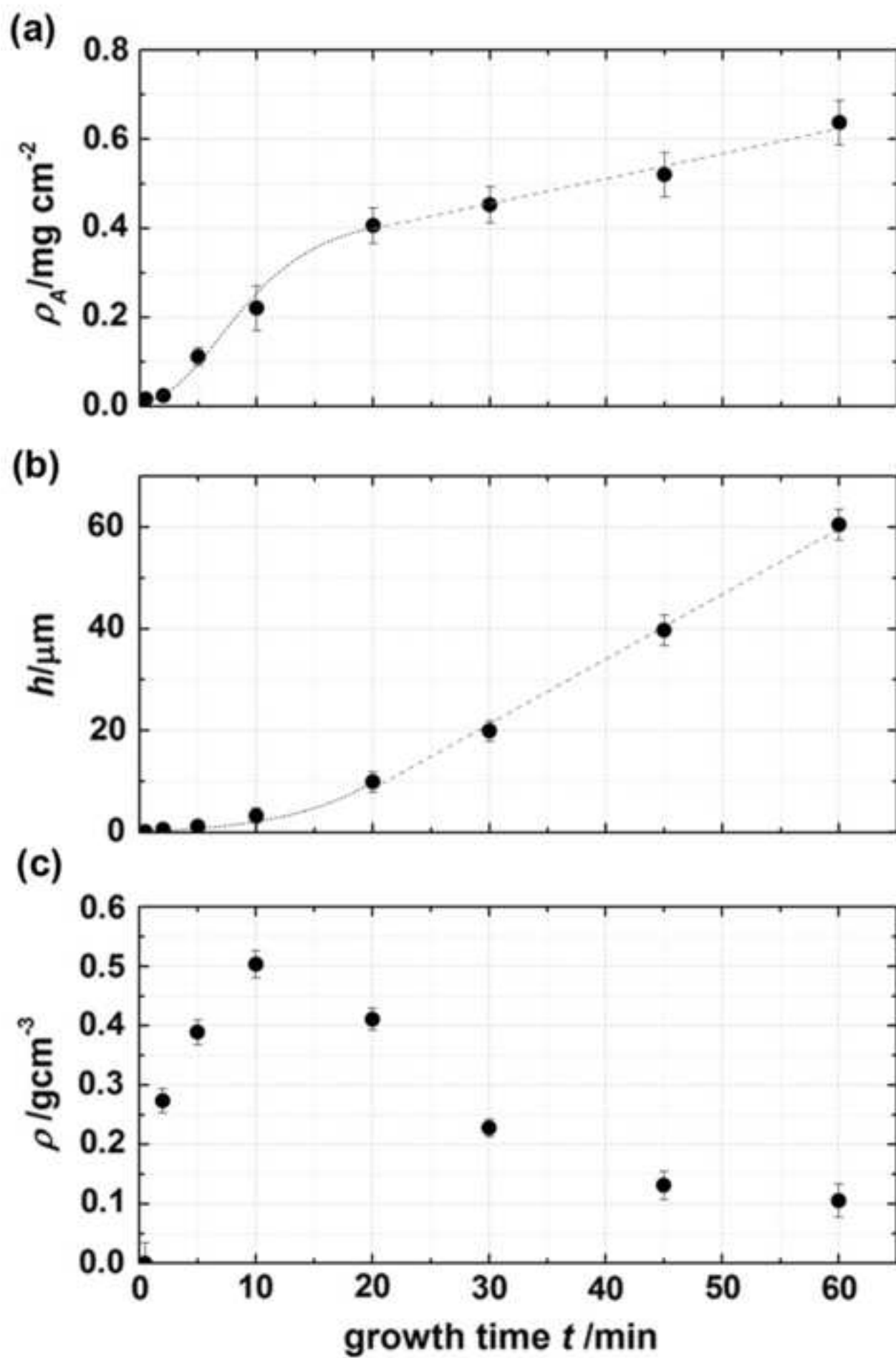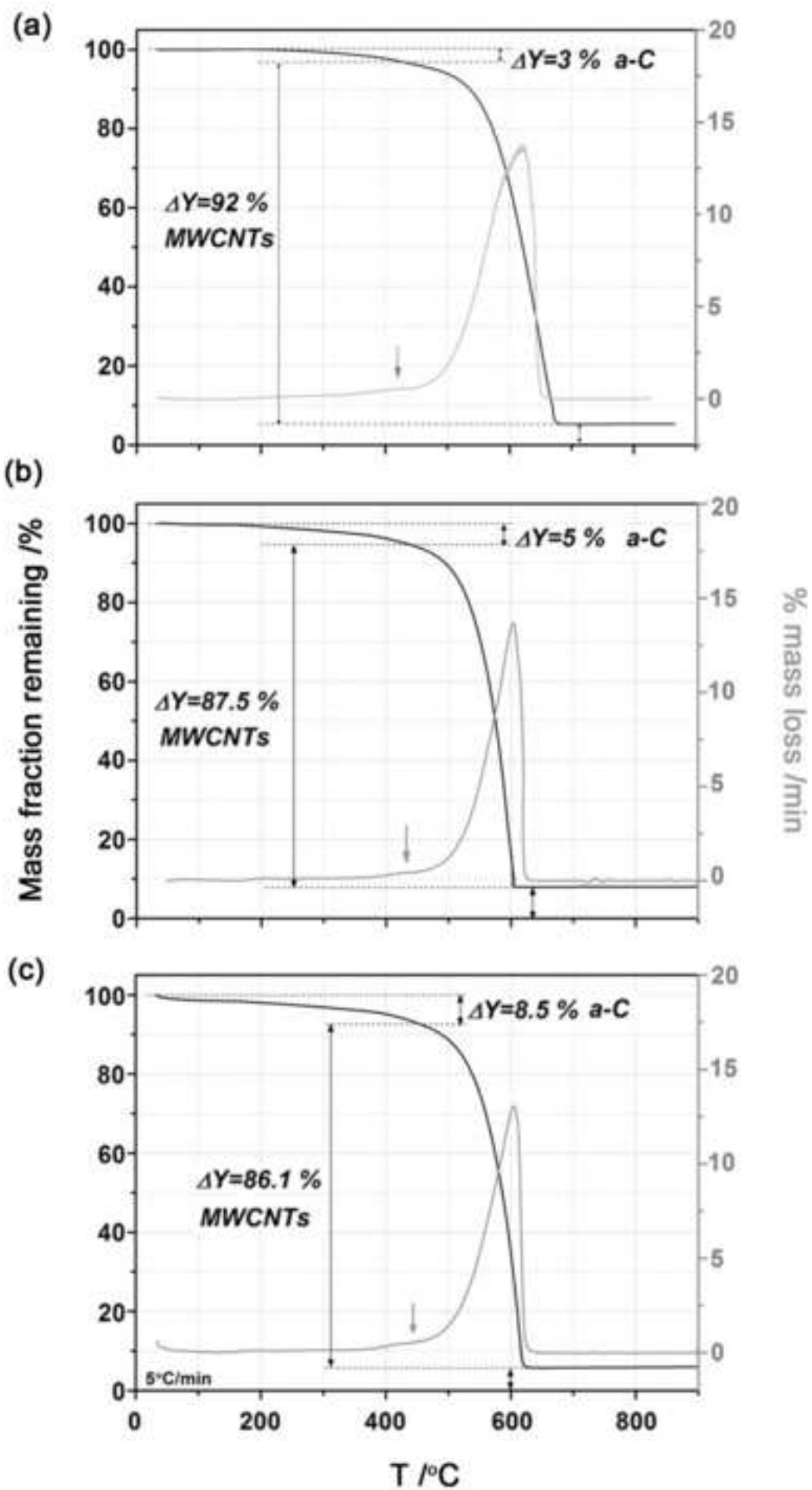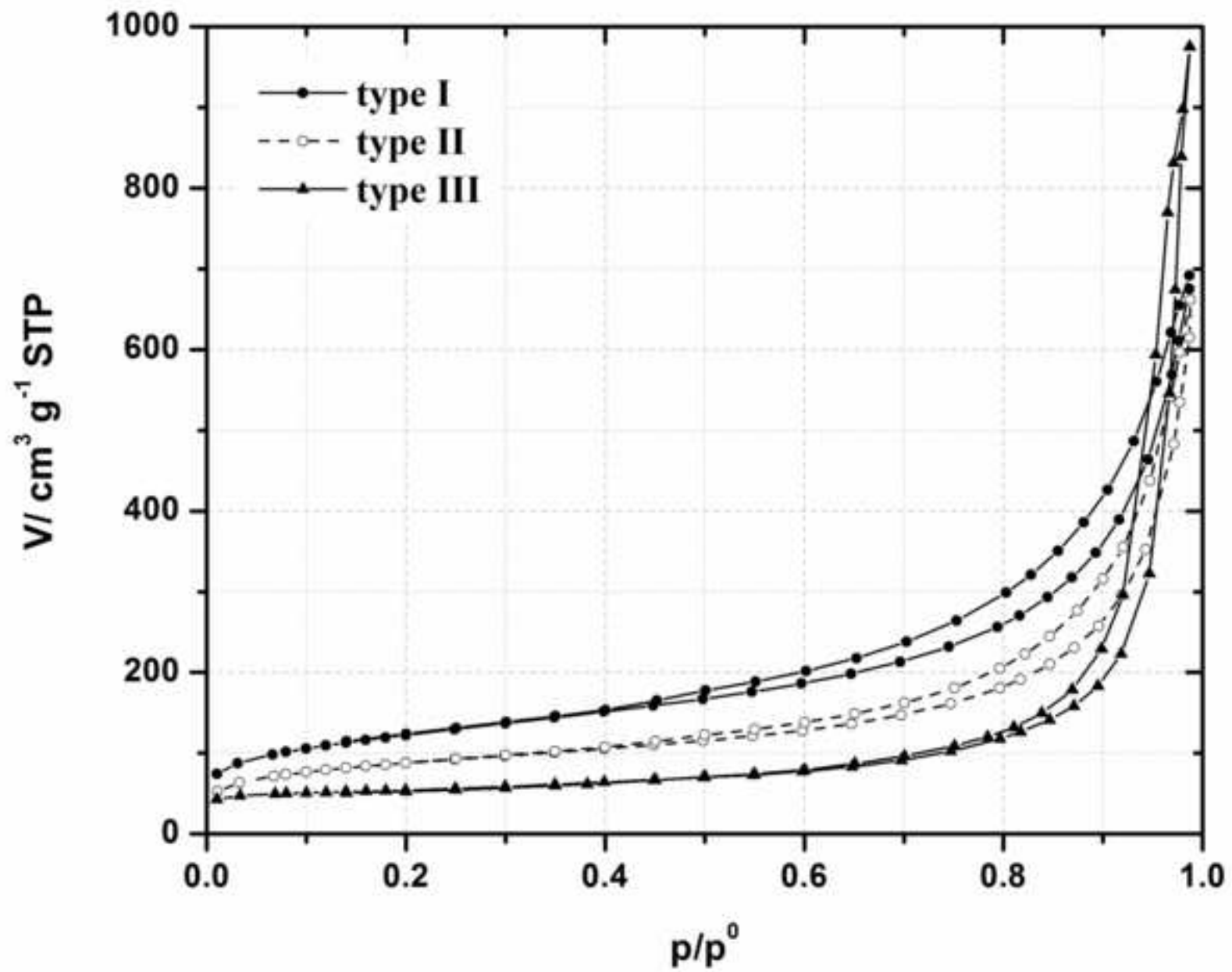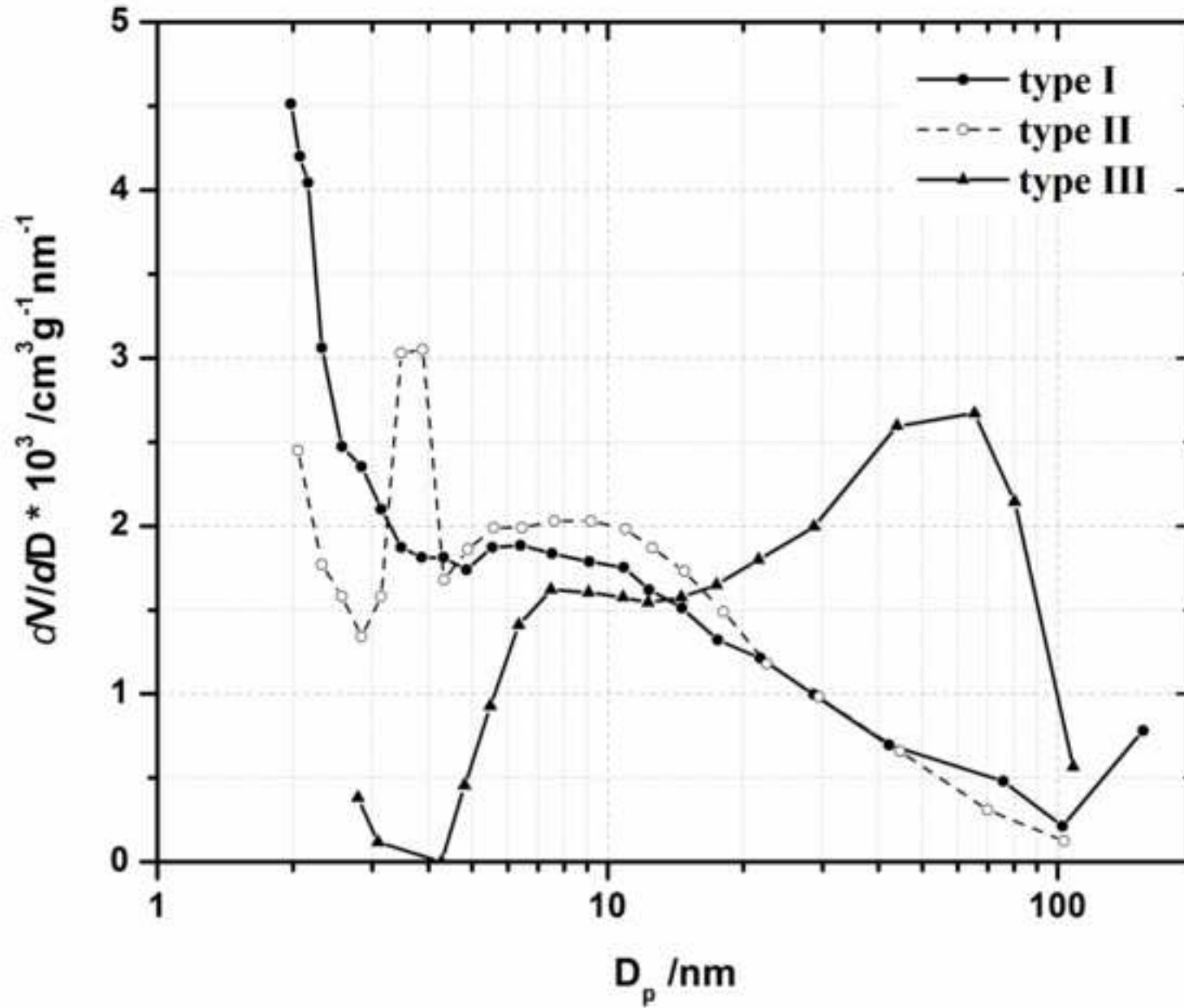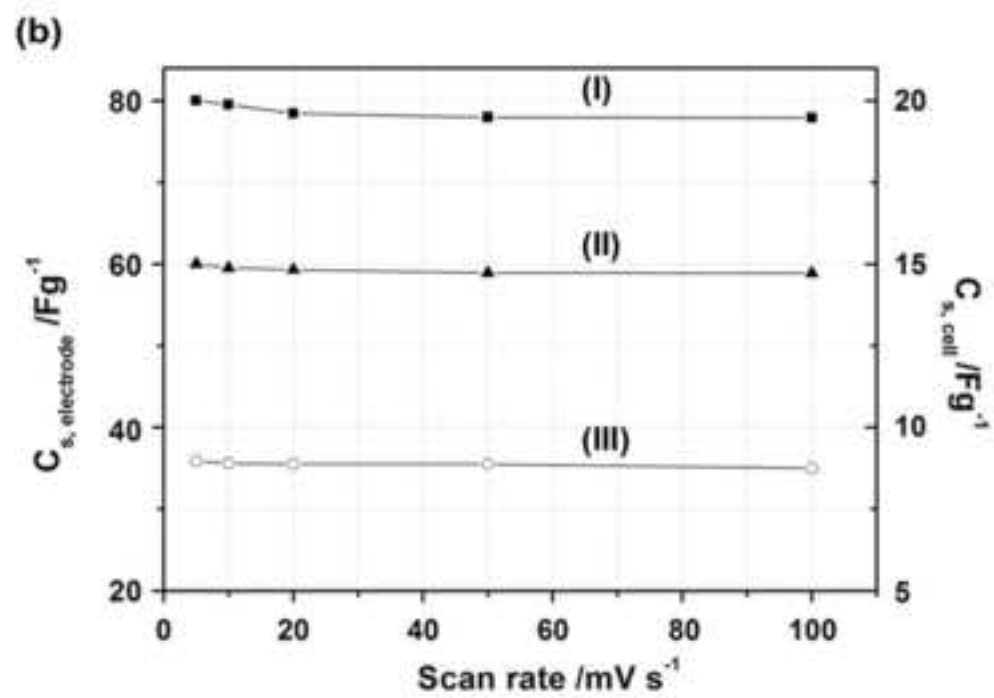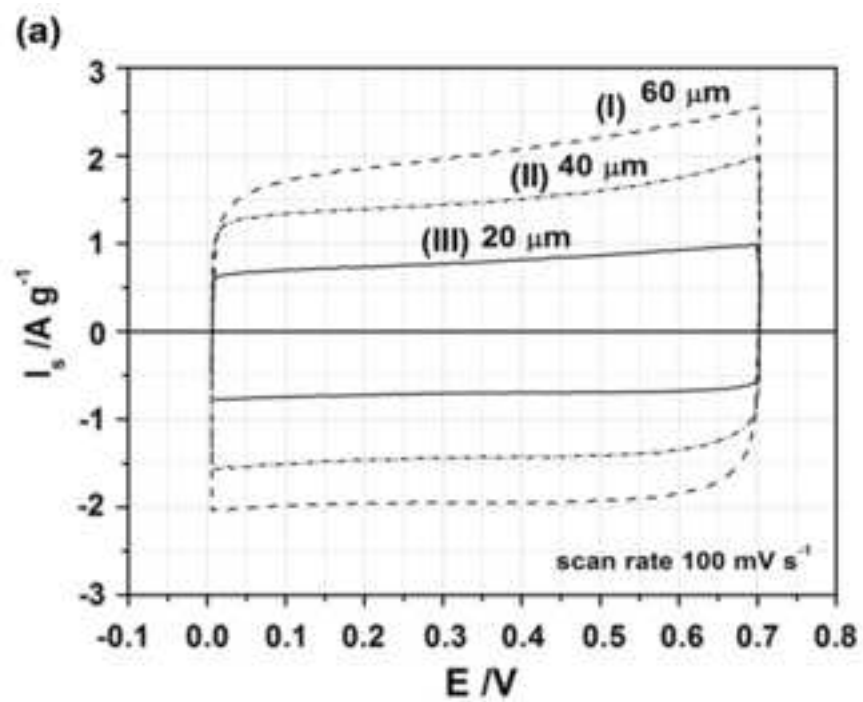
Figure 5

Figure 7

Figure 8
Click here to download high resolution image